International Journal of Nanomedicine

Dovepress
open access to scientific and medical research

Open Access Full Text Article

ORIGINAL RESEARCH

Dual-Targeted Zeolitic Imidazolate Frameworks Drug Delivery System Reversing Cisplatin Resistance to Treat Resistant Ovarian Cancer

Yan Xing[1,*], Rui Jing[2,*], Xiaoying Tang[2], Zhenqi Jiang[2]

[1]Department of Gynecology, The First Affiliated Hospital of Ningbo University, Ningbo, People's Republic of China; [2]School of Medical Technology, Beijing Institute of Technology, Beijing, People's Republic of China

*These authors contributed equally to this work

Correspondence: Zhenqi Jiang; Xiaoying Tang, Email jiangzhenqi@bit.edu.cn; xiaoying@bit.edu.cn

Objective: Ovarian cancer cells are prone to acquire tolerance to chemotherapeutic agents, which seriously affects clinical outcomes. The development of novel strategies to enhance the targeting of chemotherapeutic agents to overcome drug resistance and minimize side effects is significant for improving the clinical outcomes of ovarian cancer patients.

Methods: We employed folic acid (FA)-modified ZIF-90 nanomaterials (FA-ZIF-90) to deliver the chemotherapeutic drug, cisplatin (DDP), via dual targeting to improve its targeting to circumvent cisplatin resistance in ovarian cancer cells, especially by targeting mitochondria. FA-ZIF-90/DDP could rapidly release DDP in response to dual stimulation of acidity and ATP in tumor cells.

Results: FA-ZIF-90/DDP showed good blood compatibility. It was efficiently taken up by human ovarian cancer cisplatin-resistant cells A2780/DDP and aggregated in the mitochondrial region. FA-ZIF-90/DDP significantly inhibited the mitochondrial activity and metastatic ability of A2780/DDP cells. In addition, it effectively induced apoptosis in A2780/DDP cells and overcame cisplatin resistance. In vivo experiments showed that FA-ZIF-90/DDP increased the accumulation of DDP in tumor tissues and significantly inhibited tumor growth.

Conclusion: FA-modified ZIF-90 nanocarriers can improve the tumor targeting and anti-tumor effects of chemotherapeutic drugs, reduce toxic side effects, and are expected to be a novel therapeutic strategy to reverse drug resistance in ovarian cancer.

Keywords: ovarian cancer, drug resistance, targeted therapy, folic acid, ZIF-90, nanomedicine, mitochondria, cell apoptosis

Introduction

Ovarian cancer (OC) is one of the most lethal classes of gynecologic malignancies.[1–3] Despite advances in diagnosis and treatment, the susceptibility of ovarian cancer cells to acquire tolerance to first-line drugs remains a serious impediment to clinical outcomes.[4–6] Studies have shown that tumor cells acquire drug resistance through compliant mechanisms, such as enhanced DNA repair drug efflux, and attenuated apoptosis.[7] In particular, acquired resistance can lead to extensive tolerance of tumor cells to platinum-based chemotherapeutic agents. Cisplatin resistance has become one of the major obstacles affecting the clinical outcome of ovarian cancer.[8] Therefore, the development of novel therapeutic strategies that can bypass tumor cell surface resistance and promote drug accumulation in resistant tumor cells to reverse the resistance mechanism is significant for improving the therapeutic efficacy of ovarian cancer.

Recent studies have shown that directly targeting the internal targets of tumor cells can effectively circumvent surface resistance.[9,10] In particular, mitochondria, as the central regulatory organs of tumor cell metabolism and apoptosis, have become potential new targets for tumor therapy.[9,11,12] Back in 2013, Riganti et al[13] modified DOX (NitDOX) using NO-releasing moiety-containing modification to nitrate and inhibit mitochondria-associated ABC transporter proteins to overcome DOX resistance in cancer therapy. Cisplatin (DDP)-loaded ZIF-90 can be used to inhibit the value-added of DDP-resistant epithelial ovarian cancer cells due to its efficient pH- and ATP-responsive drug-releasing ability.[14]

Received: 20 December 2023
Accepted: 22 June 2024
Published: 3 July 2024

Mitochondria-targeted drug delivery systems can bypass the resistance mechanisms on the cell surface and directly act on mitochondrial targets, inducing apoptosis in drug-resistant tumor cells. Therefore, the development of drug carriers that can target drug delivery to tumor cell mitochondria has become a potential new strategy to overcome multidrug resistance in ovarian cancer.[15]

In recent years, the application of metal-organic frameworks (MOFs) as a novel class of drug nanocarriers has garnered widespread attention and discussion in academia.[16,17] ZIF-90 is effective in drug loading without decreasing the drug efficacy due to its biocompatibility, large porosity, and weak coordination network between its zinc ions and imidazole ring, which gives it a certain degree of structural flexibility.[18,19] More importantly, previous studies have shown that ZIF-90 can be specifically taken up into tumor cells and localized to the mitochondrial region, suggesting its potential as a mitochondrial-targeting carrier. Pan et al[20] proposed a mitochondrial ATP-triggering strategy for nanoscale ZIF-90, whereby ZIF-90 is targeted to cancer cells through the interaction of mutual electrostatic interactions on their surfaces as well as the competitive coordination between Zn mitochondria, and a strategy that utilizes mitochondrial adenosine triphosphate (ATP) to break down ZIF-90 to release the drug. In addition, the presence of functional groups such as aldehyde groups on the surface of ZIF-90 enables the modification of various targeting ligands through simple covalent linkages, further enhancing its targeting of tumor cells, especially drug-resistant cells.[21,22] Inspired by this idea, we believe that folic acid (FA) can be coupled with ZIF-90 as a molecular targeting device, which can not only target the folate receptors overexpressed on cancer cells but also facilitate the accumulation of the nanocarrier in the mitochondrial region. This FA-coupled dual-targeting strategy is expected to bypass the resistance mechanisms and improve tumor therapeutic efficacy by overcoming cisplatin resistance.

This study aims to construct an innovative FA-ZIF-90/DDP nanosystem using a one-pot preparation strategy to achieve dual-targeted delivery to ovarian cancer cells and their mitochondria and overcome cisplatin (DDP) resistance. The system combines the structural advantages of ZIF-90 nanocarrier with the biological targeting of folic acid (FA). The Introduction of FA enhances the specific binding between the carrier and the folate receptor overexpressed on the surface of tumor cells and promotes the enrichment of the carrier inside the cells, particularly in mitochondrial regions. This study focuses on systematically comparing the differences in tumor targeting, cytotoxicity, and pharmacokinetics of ZIF-90 nanocarriers before and after FA modification to verify the efficacy of the folic acid modification strategy in enhancing the tumor targeting of the ZIF-90 system and to evaluate its biological safety. At the same time, this study will demonstrate the potential of FA-ZIF-90/DDP in overcoming drug resistance, improving drug delivery efficiency, and reducing side effects. In a word, this study systematically evaluated the effect of folic acid modification on enhancing the tumor targeting of the ZIF-90 nanocarriers delivery system by the FA-ZIF-90/DDP nano platform. It provided a reference for the design and optimization of ZIF nanodrugs, to achieve a breakthrough in the treatment of drug-resistant ovarian cancer in the field of precision medicine.

Experimental Component

A2780/DDP Cell Culture

The cisplatin-resistant human ovarian cancer cell line A2780/DDP was obtained from Shanghai Aolu Co. Ltd. (Shanghai, China). The cells were maintained in RPMI-1640 medium supplemented with 10% fetal bovine serum and 1% penicillin-streptomycin at 37°C in a humidified atmosphere containing 5% CO2. The cells were passaged every 2–3 days, and the cells in the logarithmic growth phase were taken for subsequent experiments. To maintain DDP resistance in A2780/DDP cells, 1 μg/mL DDP was added to the culture medium at each passaging to pretreat the cells for 48 h, after which the medium was replaced with a drug-free medium to continue the culture. The stable tolerance of A2780/DDP cells to DDP was periodically verified using CCK-8 cell viability assay. One day before each cell experiment, A2780/DDP cells in the logarithmic growth phase were collected by digestion with 0.25% trypsin, counted and recovered, resuspended in a complete medium at the desired density, and routinely cultured overnight for subsequent experiments.[23] All cell cultures were carried out in a sterile environment free of contamination with penicillin.

Synthesis of Nanomaterials

Preparation of ZIF-90@DDP and FA-ZIF-90@DDP: First, ZIF-90@DDP nanoparticles were synthesized. Typically, every 2 mL of $Zn(NO_3)_2$–$4H_2O$ (0.1 M) and 2 mL of 2-ICA (0.2 M) were mixed with 5 mg/mL DDP in DMF. Within 5 min of the start of the reaction, 10 mL of DMF was added and stirred for 20 min. The mixture was washed with DMF and methanol by centrifugation and then dried under vacuum for 12 h at room temperature and stored at 4°C protected from light. To synthesize FA-functionalized ZIF-90@DDP (FA-ZIF-90@DDP), 20 mg of folic acid (FA) was dissolved in 25 mL of methanol in a 10 mL round-bottom flask, followed by addition of 50 mg of ZIF-90@DDP. The mixture was allowed to react for 48 hours before centrifugation at 10,000 rpm for 10 minutes. The resulting pellet was washed repeatedly with methanol to remove unreacted reagents and ligands. Finally, the FA-conjugated product FA-ZIF-90@DDP was collected and dried under vacuum for 12 hours at room temperature.

Preparation of ZIF-90/RhB and FA-ZIF-90/RhB: DDP was replaced with Rhodamine B (RhB), and the rest of the steps were the same as above.

Characterization of FA-ZIF-90

The FA-ZIF-90 nanoparticles were collected characterized and analyzed by transmission electron microscopy (TEM), powder X-ray diffractometer (XRD), dynamic light scattering (DLS), and infrared spectrometry (IR) to confirm the physicochemical properties of synthesized FA-ZIF-90 nanoparticles, such as morphology, crystal structure, particle size distribution, and surface modification.

In vitro Drug Release

1 mg of FA-ZIF-90@DDP and ZIF-90@DDP nanoparticles were taken and dispersed in 1 mL of PBS buffer at pH 7.4 and pH 5.5 respectively, and placed on a 37°C water bath shaker. 0.1 mL of the gradient buffer samples were removed at preset time points (0, 0.5, 1, 2, 4, 8, 12 h), and the filtrate was obtained by centrifugation (MWCO 20 kDa) in an ultrafiltration tube. The DDP content in the filtrate was detected using coupled plasma-optical emission spectrometry (ICP-OES). The in vitro cumulative release curves of the two carriers at different pH conditions were plotted to compare the differences in drug release behavior.

Drug release experiments were also designed to simulate the ascites environment in vitro: 1 mg of FA-ZIF-90@DDP nanoparticles was taken and dispersed in 1 mL of PBS buffer (containing 10% fetal bovine serum) at pH 5.5 and subjected to 37°C oscillation. The remaining steps were as above.

Evaluation of drug release behavior of FA-ZIF-90@DDP in acidic and high ATP environments that are easily activated by tumor cells: 1 mg of FA-ZIF-90@DDP nanoparticles was dispersed in 1 mL of PBS buffer (containing 2 mM ATP) at pH 5.0, and subjected to shaking at 37°C. The remaining steps were as above. The remaining steps were as above.

Hemosolubility

Different concentrations of FA-ZIF-90 nanoparticle aqueous solutions (0.5, 1, 2, 4, 8 μg/mL) were taken in 100 μL each, and added into 96-well plates, with three replicate wells in each group. Add 100 μL of fresh mouse erythrocyte suspension to each group, and set up the positive control group (add deionized water) and negative control group (add PBS buffer). The sample was gently shaken and incubated at 37°C for 8 h. After centrifugation at 3000 rpm for 5 minutes, the supernatant was collected and the optical density (OD) at 540 nm was measured to quantify the released hemoglobin. The percentage hemolysis was calculated for each sample using the following equation:

Hemolysis rate = [(OD value of experimental group - OD value of negative control group)/ (OD value of positive control group - OD value of negative control group)] x 100%

Plot the hemolysis curves of erythrocytes with different concentrations of FA-ZIF-90 nanoparticles. Derive the final hemolysis rate data to evaluate the hemocompatibility of FA-ZIF-90 nanoparticles.

Internalization of Nanoparticles

Detection of cell phagocytosis by flow cytometry: A2780/DDP cells in the logarithmic growth phase were taken and the density was adjusted to 2×10^5 cells/mL. 1 mL of cell suspension was taken and mixed with 1 mL of FA-ZIF-90/RhB suspension at a concentration of 100 μg/mL and 1 mL of ZIF-90/RhB suspension at a concentration of 100 μg/mL respectively, and placed in an incubation incubator. 100 μL of each sample was taken into a flow-through tube at different time points (0h, 1h, 2h, 4h, 8h), resuspended with 1 mL of pre-cooled PBS, and incubated for 30 min at 4°C, protected from light. 3000 rpm centrifugation was performed for 5 min to discard the supernatant, and the precipitate was resuspended in 0.3 mL of PBS for the flow-through assay. The fluorescence intensity detected by the FITC channel was recorded to plot the cellular phagocytosis of the two nanoparticles at different time points.

Intracellular and mitochondrial drug detection: A2780/DDP cells in the logarithmic growth phase were taken and inoculated in 6-well plates at a density of 2×10^5 cells/mL and cultured until the cells were adherent to the wall. ZIF-90@DDP suspension and FA-ZIF-90@DDP suspension at a concentration of 10 μg/mL were added at 2 mL/well respectively, and cultured for 2 h and 8 h. After centrifugation, the supernatant was removed and the cell pellet was resuspended and washed twice in phosphate buffered saline (PBS) to remove residual media and unattached nanoparticles. Add lysis solution 300 μL/well, lysis on ice for 30 min, and collect the extracts. The extracts were subjected to inductively ICP-OES analysis to determine the platinum content, which represents the intracellular DDP levels. The BCA method was used to determine the protein content for normalization of DDP levels. Another portion of cells was taken for mitochondrial extraction the mitochondrial extracts were similarly analyzed by ICP-OES to quantify the DDP levels in mitochondria.

Confocal detection of mitochondrial targeting: A2780/DDP cells were spread on slides and left to attach to the wall. Add FA-ZIF-90/RhB suspension and ZIF-90/RhB suspension at a concentration of 100 μg/mL each 0.5 mL/slice, respectively, and incubate for 2 h and 8 h. Discard the supernatant and wash with PBS. Add diluted DAPI and Mito Tracker Green 100 μL/slice each for labeling. The distribution of red fluorescence of RhB from different treatments was observed and recorded under the fluorescence microscope.

Cellular Mitochondrial Interference and Cell Migration

Mitochondrial membrane potential was detected by flow cytometry: A2780/DDP cells in the logarithmic growth phase were collected, the density was adjusted to inoculate in 6-well plates, 1×10^5 cells were added to each well, and cultured overnight until the cells completely adhered to the wall. On the next day, the medium was aspirated and discarded, and different treatments were gently added to each well, including: PBS 2 mL/well, DDP solution at a concentration of 1 μg/mL with 2 mL/well, ZIF-90@DDP suspension at a concentration of 1 μg/mL DDP with 2 mL/well, and FA-ZIF-90@DDP suspension at a concentration of 1 μg/mL DDP with 2 mL/well respectively. The well plates were placed in an incubator to continue incubation for 24 h. After 24 h, the supernatant of each well was aspirated and washed twice with PBS. Add 0.25% trypsin 200 μL/well to each well, incubate for 3 min to fully disperse the cells, and add medium containing 10% fetal bovine serum to terminate the digestion. The cell suspension of each well was collected and transferred to a flow-through tube, centrifuged at 1000 rpm for 5 min, and the supernatant was discarded. Add 100 μL of JC-1 working solution to the precipitate, mix thoroughly, and incubate for 20 minutes away from light. Add 1 mL of flow buffer and mix well. The fluorescence intensity of the samples in each tube was detected by flow cytometry. Finally, the cellular mitochondrial membrane potential scatter plots were plotted and other analyses were performed.

Confocal detection of mitochondrial activity: A2780/DDP cells in the logarithmic growth phase were taken and inoculated on slides at a density of 1×10^5 cells/mL, and placed in an incubator overnight to allow the cells to be completely adhered to the wall. The following day, non-adherent cells were aspirated and discarded, and different treatments were gently added, including: PBS 0.5 mL/slice, 1 μg/mL DDP solution at a concentration of 1 μg/mL DDP with 0.5 mL/slice, 1 μg/mL ZIF-90@DDP suspension 0.5 mL/slice, and 1 μg/mL DDP of FA-ZIF-90@DDP suspension 0.5 mL/slice. The incubation was continued for 24 h and then each treatment was discarded and washed twice with PBS. Then Mito Tracker Green solution at a concentration of 10 μM was added 100 μL/slice to each slice and incubated for 30 min away from light for mitochondrial activity labeling. After that, PBS was washed 3 times to remove unabsorbed reagents. Finally, the fluorescence emission spectra in the range of 460–480 nm and 500–545 nm were detected under

a preheated confocal laser scanning microscope with excitation at 405 nm and 488 nm, respectively. The fluorescence intensities of normal and damaged mitochondria in different treatment groups were recorded to evaluate the effects of different treatments.

Cell migration was evaluated by cell scratch assay: A2780/DDP cells in the logarithmic growth phase were taken and inoculated in 6-well plates at a density of 2×10^5 cells/mL, and incubated overnight at 37°C in an incubator until the cells were completely attached to the wall. Two straight lines were drawn parallel to the bottom of each well with an extracting fat pen, with a uniform line and a line width of about 1 mm. PBS was washed to remove the detached cells produced during the scratching. Then different treatments were added to each well respectively, including: PBS 2 mL/well, DDP solution at a concentration of 1 μg/mL DDP with 2 mL/well, ZIF-90@DDP suspension at a concentration of 1 μg/mL DDP with 2 mL/well, FA-ZIF-90@DDP suspension at a concentration of 1 μg/mL DDP with 2 mL/well. Then the cells were continued to be incubated in the incubator for 24 h. Cell migration and wound healing were recorded by taking pictures in the same field of view at the time points of 0h and 24h after scratching.

Counting the number of migrated cells: Using confocal microscopy, the number of migrated cells in each treatment group was photographed and recorded under the same preset field of view. The relative number of migrated cells in each treatment group was calculated using the number of migrated cells in the PBS-treated group as a standard. Finally, bar graphs were drawn to evaluate the effects of different treatments on the migration ability of A2780/DDP cells.

Cytotoxicity

CCK-8 assay for cell viability: logarithmic growth phase A2780/DDP cells were collected and homogeneously inoculated in 96-well plates after adjusting the cell density to 5×10^4 cells/mL by cell counting plate. Different concentrations of FA-ZIF-90@DDP and ZIF-90@DDP were added respectively, where the concentrations of DDP for FA-ZIF-90@DDP and ZIF-90@DDP were 0.1 to 2 μg/mL. A 24-hour treatment was performed. Set up a control group (medium containing cells only). Add CCK-8 solution (5% 10 μL). Detect the OD value of each well using an enzyme marker. The cytotoxic effects of the two nanomaterials on A2780/DDP cells were evaluated and compared by plotting cell viability curves.

Detection of apoptosis by flow cytometry: logarithmic growth phase A2780/DDP cells were collected and treated by adding mL of PBS, DDP, ZIF-90@DDP and FA-ZIF-90@DDP (DDP: 1 μg/mL) for 24 h, respectively. The DDP concentration of 1 μg/mL was chosen as it falls within the half-maximal inhibitory range based on the 24 h Cytotoxicity assay, allowing for effective evaluation of cytotoxicity differences between formulations. Cell labeling was performed using PI and Annexin V-FITC double staining. The apoptosis rate of cells in each group was detected by flow cytometry.

Fluorescence microscope observation of apoptosis: After 24 hours of treatment A2780/DDP cells were cultured on slides and labeled with membrane-associated proteins and nuclear DNA, respectively. Membrane-associated protein V-FITC (green) was used for labeling the cell membrane-associated proteins, and PI (red) was used for labeling the nuclear DNA of apoptotic cells. The 24 h treatment duration and 1 μg/mL DDP concentration were chosen to maintain consistency with other cytotoxicity experiments for better data correlation. Fluorescence localization was carried out to observe apoptosis of the cells in each treatment group. By fluorescence microscopy, normal cells should show green fluorescence and apoptotic cells show red fluorescence in different treatment groups. The changes in fluorescence intensity of normal cells (green) and apoptotic cells (red) under different treatments were recorded and analyzed. In the course of observation, images were captured for subsequent further analysis.

A2780/DDP Human Ovarian Cancer Tumor Xenograft Establishment

The experimental steps to establish the A2780/DDP human ovarian cancer tumor model followed the protocol approved by the Beijing Institute of Technology (Permit No. SYXK Jing 2017–0031) and under the guide of Guide for the Care and Use of Laboratory Animals (Washington (DC): National Academies Press (US); 2011). Four- to six-week-old Balb/C nude mice, which were purchased from Sibeifu Biotechnology Co., Ltd (Beijing, China), were used as experimental animals. First, the culture of A2780/DDP cells was performed to ensure their good growth status. Then, 1×10^7 cells were suspended in 100 μL of appropriate medium and the cell suspension was injected into the back of each Balb/C nude mouse by subcutaneous injection. Tumor growth was measured periodically and tumor volume was calculated. Tumor

volume = a × b^2/2 (a = tumor length, b = tumor width). At the end of the experiment, relevant data or tissue samples were collected for subsequent analysis according to the experimental design.

Evaluation of in vivo Distribution

A2780/DDP bearing nude mice were randomly divided into 4 groups (n=5) and injected with different agents (PBS, DDP, ZIF-90@DDP, FA-ZIF-90@DDP) via tail vein. After 4 weeks of continuous drug administration, peripheral blood cytological indices were collected and tested using a hematology analyzer and an autoanalyze. The mice were executed, and heart, liver, spleen, and kidney tissues were collected, and the Pt content in the tissues was detected by ICP-MS after acid digestion to assess the distribution and accumulation of Pt in major organs.

In vivo Anti-Tumor Efficacy

A Tumorigenic A2780/DDP bearing nude mice model was used, and when the tumor volume reached 60–80 mm^3, 4 groups (n=5) were randomly divided into 4 groups, and different preparations (PBS, DDP, ZIF-90@DDP, FA-ZIF -90@DDP, A administered at a dose of 5 mg/kg) were injected via tail vein, respectively. The drugs were administered continuously for 2 weeks, the tumor's long and short diameters were measured every 2 days, and the volumes were calculated to plot the growth curves. The relative tumor growth inhibition rate of each treatment group was finally calculated. At the same time, the body weight was weighed every 2 days and the weight change curve was plotted. After finishing the drug administration, the survival time and survival curve of mice were observed and recorded. Finally, the mice were executed, and the tumor tissues and major organs were quickly collected for H&E staining, TUNEL apoptosis detection, Ki67 detection, etc., and examined with an optical microscope (DMI3000, Leica, Germany).

In vivo Safety Evaluation

At the end of the in vivo anti-tumor experiments, the mice were executed, and the main organs such as the heart, liver, spleen, and kidney were quickly collected. Paraffin sections were prepared according to the standards of histopathology experiments, H&E stained, and the histopathological changes of each organ were observed under a light microscope (DMI3000, Leica, Germany) (400x). The arrangement of cardiomyocytes, the structure of liver lobules, the distribution of white versus red splenic medulla of the spleen, and the morphology of renal tubules and glomeruli in different administration groups were recorded. The organ toxic effects of different nanoformulations were evaluated in comparison with the PBS normal control group.

Statistical Analysis

Statistical analysis was performed by one-way analysis of variance (ANOVA) followed by student testing using SPSS 18.0 software. All statistical differences were calculated using an unpaired two-tailed Student's *t*-test with GraphPad Prism 9.0 (GraphPad Software, Inc., CA, USA). Statistically significance was set ns (not significantDP), *p < 0.05 (significant), **p < 0.01 (moderately significant), and ***p < 0.001 (highly significant).

Results and Discussion

Characterization, Drug Release, and Blood Solubility of FA-ZIF-90

In the precursor experiments, we synthesized ZIF-90 by the room temperature colloidal chemical pathway and measured the particle size of ZIF-90 to be 85 ± 8 nm and the hydrated particle size to be 105.8 ± 7.5 nm.[14] FA-ZIF-90/DDP was synthesized by room temperature coupling folic acid (FA) on the surface of ZIF-90/DDP obtained in a one-pot method.[24] Transmission electron microscopy (TEM) revealed that the FA-functionalized ZIF-90/DDP nanoparticles (FA-ZIF-90/DDP) were spherical in shape with an average diameter of 60 ± 10 nm (Figure 1a). Dynamic light scattering (DLS) measured the hydrodynamic size of FA-ZIF-90/DDP to be 110 ± 10.6 nm (Figure 1b). The surface charge, quantified by zeta potential, was determined to be −5.7 ± 0.7 mV. Powder X-ray diffraction (PXRD) analysis confirmed the successful synthesis of crystalline FA-ZIF-90/DDP nanoparticles (Figure 1c), and the synthesized nanomedicine maintained the similarity with the results of the previous ZIF-90 crystal structure study.[21] The IR spectral characteristics of ZIF-90 and

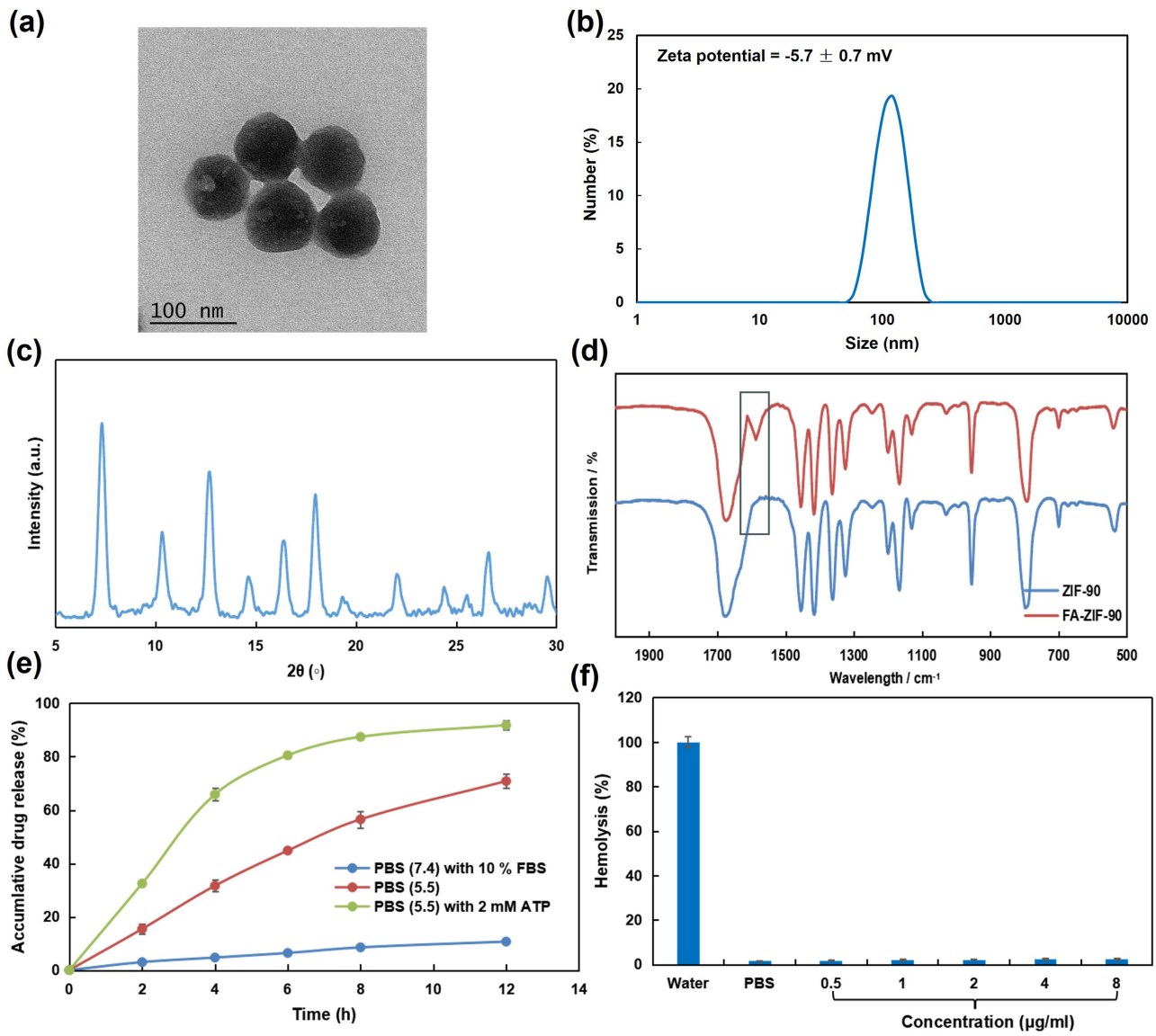

Figure 1 Preparation, material characterization, drug release, and hemolysis of FA-ZIF-90/DDP. (**a**) TEM image of FA-ZIF-90/DDP. (**b**) DLS analysis of FA-ZIF-90/DDP in PBS. (**c**) XRD images of FA-ZIF-90/DDP. (**d**) IR spectra of ZIF-90 and FA-ZIF-90. (**e**) The in vitro cumulative release profiles of cisplatin (DDP) from the FA-conjugated ZIF-90@DDP nanoparticles (FA-ZIF-90@DDP) were determined over 12 hours at 37°C in PBS at pH 7.4, 5.5, 5.5 with 10% fetal bovine serum (FBS), and 5.0 with 2 mM adenosine triphosphate (ATP). (**f**) Hemosolubility in WATER, PBS, and samples of different concentrations (0.5, 1, 2, 4, and 8 μg/mL). Data represent the mean ± SD (n=3).

FA-ZIF-90 were further investigated in comparison (Figure 1d). The results showed that a characteristic peak at 1600/cm-1 wavelength was observed for FA-ZIF-90, which could be caused by the change of the functional groups of ZIF-90 after coupling FA, and confirmed the successful modification of FA on the surface of ZIF-90.[25] To investigate whether FA modification alters the in vivo drug release behavior of ZIF-90 as a drug carrier, we examined the cumulative drug release studies of FA-ZIF-90 particles loaded with DDP under pH and ATP conditions that mimic different in vivo environments (Figure 1e). FA-ZIF-90@DDP exhibited pH- and ATP-dependent drug release patterns under different pH and ATP conditions. The overall results showed that the addition of ATP as a "pro-degradant" could enhance the drug release from the particles under acidic conditions. Meanwhile, the acidic condition facilitated the drug release from FA-ZIF-90@DDP, while the physiological pH 7.4 condition did not actively release the drug, which is similar to the drug release pattern of ZIF-90 nanocarrier platforms reported previously.[21,26] We further evaluated its biosafety as a carrier for drug delivery, ie, we compared the hemolysis of erythrocytes with different concentrations of FA-ZIF-90 aqueous solution and PBS buffer solution (Figure 1f). Among them, the pure water (positive control) group showed a high

degree of hemolysis close to 100%. While all FA-ZIF-90 concentration groups showed a safety of less than 5% hemolysis in PBS buffer. This result indicated that FA-ZIF-90 showed good biosafety and hemocompatibility under physiological conditions compared with the positive control purified water group, and the hemolysis rate increased slightly with increasing concentration but remained at an acceptable level. In conclusion, FA-ZIF-90@DDP synthesized by ZIF-90@DDP coupled to FA can promote the rapid release of DDP in the acidic and high ATP environment of tumor cells and does not cause significant damage to erythrocytes in the in vivo environment, which proves its good potential for in vivo application.

Cellular Phagocytosis of FA-ZIF-90

Numerous studies have demonstrated overexpression of the folate receptor (FR) on the surface of ovarian cancer cells. This receptor specifically binds to folic acid (FA) and mediates intracellular transport into the mitochondria.[27–29] To verify the enhanced cellular targeting by FA modification, we compared the cellular endocytosis of two materials, FA-ZIF-90/RhB, and ZIF-90/RhB, using the flow cytometry technique. Among them, the half-maximal inhibitory concentration (IC50) values of DDP in A2780/DDP cells used in this experiment were 2.5–3.2-fold higher than those in the parental cells of A2780, the former of which was confirmed to be a drug-resistant lineage cell.[30] The FA-ZIF-90/RhB nanoparticles with targeting moiety FA and ZIF-90/RhB nanoparticles without targeting moiety phagocytosis by human ovarian cancer cisplatin-resistant cells (A2780/DDP) at different time points (0h, 1h, 2h, 4h, and 8h) were shown (Figure 2a and b). The results demonstrated a time-dependent increase in fluorescence intensity for both samples, indicating gradual uptake of the nanoparticles by the cells over time. This suggests that cellular internalization of the nanoparticles was increased with longer incubation periods. After 8 hours of incubation, the fluorescence intensity of the FA-conjugated ZIF-90/RhB nanoparticles was over 10 times higher compared to the non-targeted ZIF-90/RhB group. This significant enhancement verifies that functionalization with folic acid (FA) drastically improved the intracellular uptake of the nanoparticles in the ovarian cancer cells. It has been demonstrated that the presence of multiple FA transporter proteins in the cell membrane of ovarian cancer cells mediates the uptake of FA, which can bind non-covalently to intracellular binding proteins after it enters the cell, protect folic acid from intracellular degradation, and mediate its transportation to the mitochondria.[31–33] To further validate the effect of FA modification on the targeted delivery of drug-carrying nanoparticles, we examined the changes in Pt concentration of FA-ZIF-90@DDP and ZIF-90@DDP nanoparticles in A2780/DDP and mitochondria (Figure 2c). The results showed that compared with the ZIF-90@DDP group, the platinum concentration in cells and mitochondria in the FA-ZIF-90@DDP group increased by 1.5 times and 1.7 times at 2h and 8h respectively. The trend of platinum concentration changes in mitochondria in both groups was consistent with the overall intracellular changes. Based on the above results, we compared the intracellular localization of different nanoparticles using confocal fluorescence microscopy (Figure 2d and e). RhB was co-loaded in ZIF-90 and FA-ZIF-90, and nuclear fluorescence (DAPI, blue), mitochondrial fluorescence (Mito Tracker Green, green), and RhB fluorescence (Rhodamine B, red) were used to visualize cellular uptake. The results showed that all four fluorescence intensities gradually increased with time after co-incubation of FA-ZIF-90@RhB and ZIF-90@RhB with A2780/DDP cells, respectively, indicating an increase in the amount of drug nanoparticles entering the cells and mitochondria.FA-ZIF-90@RhB showed brighter red fluorescence as compared to ZIF-90@RhB, indicating that FA -ZIF-90@RhB had a higher cellular uptake efficiency.

In summary, the above experiments accurately demonstrated the intracellular internalization pathways and specific processes, which not only confirmed that drug-carrying FA-ZIF-90 could be efficiently uptaken by the nucleus and mitochondria and that the precise release of the drug led to cell death, but also provided the basis for the experimental results of intracellular transport of drug carriers.

Effect of FA-ZIF-90 on Cellular Mitochondrial Interference and Cell Migration

Mitochondria play a critical role in regulating metabolism and apoptosis in cancer cells. Prior evidence indicates that folic acid-conjugated nanomaterials can selectively target mitochondria in tumor cells and disturb their energy metabolism. By accumulating in mitochondria, the FA-modified nanoparticles can interfere with the metabolic pathways and energy production.[34–36] To assess the effect of FA modification on cellular mitochondrial function in this study, we

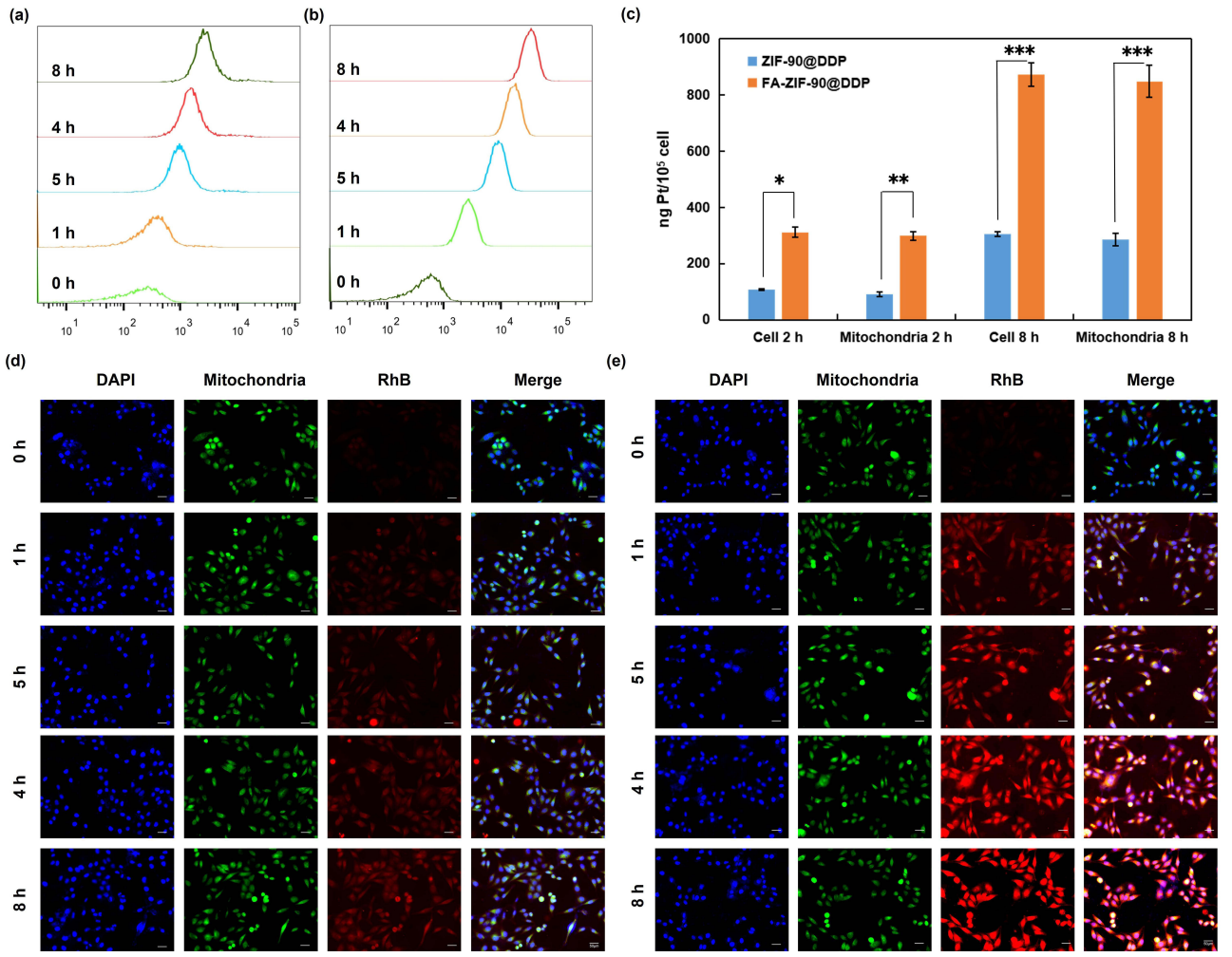

Figure 2 In vitro study of FA-ZIF-90 and ZIF-90 nanomaterials uptake by human ovarian cancer cisplatin-resistant cells (A2780/DDP). (**a** and **b**) Flow cytometry analysis of internalization of ZIF-90/RhB and FA-ZIF-90/RhB nanoparticles by A2780/DDP cells over time. (**c**) Cytosolic and mitochondrial accumulation of ZIF-90/RhB and FA-ZIF-90/RhB nano system corresponding to 2 h and 8 h of incubation in A2780/DDP cells respectively. (**d**) A2780/DDP cells over time uptake of ZIF-90/RhB confocal fluorescence micrographs and (**e**) FA-ZIF-90/RhB confocal fluorescence micrographs (Scale bar = 50 μm). Data from ICP-OES represent the mean ± SEM of three independent experiments. Statistical significance among groups: *P < 0.05, **P < 0.01, ***P<0.001.

analyzed the inhibitory effect of FA-ZIF-90 on cellular mitochondrial membrane potential by flow cytometry after JC-1 staining (Figure 3a). In the control group, cellular mitochondria were mainly distributed in the Q2 region of the normal state (93.9%), whereas most of the mitochondria in the FA-ZIF-90@DDP-treated group were shifted to the Q3 region (77%), suggesting a decrease in mitochondrial activity. Compared to the cisplatin group (6.53% in Q3) and the ZIF-90@DDP group (53.3% in Q3), FA-ZIF-90@DDP caused more mitochondria to enter into the damaged state. This suggests that FA-modified ZIF-90 can induce apoptosis by inhibiting mitochondrial activity more significantly through its mitochondrial targeting effect compared with ZIF-90. To further visualize the effect of FA-ZIF-90 on mitochondrial activity in A2780/DDP cells, confocal microscopy was used to compare the changes in intracellular fluorescence signals after different nanoparticle treatments (Figure 3b). The control group showed strong green and weak red fluorescence, indicating normal activity. With the change of treatment groups, the red fluorescence gradually enhanced while the green fluorescence weakened, indicating a decrease in mitochondrial activity, with the most significant effect in the FA-ZIF-90@DDP group. This confirms that the two nanocarriers can inhibit mitochondrial activity to different degrees, while FA-modified ZIF-90 can achieve more effective mitochondrial inactivation through targeting. The mechanism may be that FA modification can be targeted into mitochondria and release more DDP, directly inhibiting mitochondrial respiratory chain activity.[37,38] Based on the above results that FA-ZIF-90@DDP significantly inhibits mitochondrial

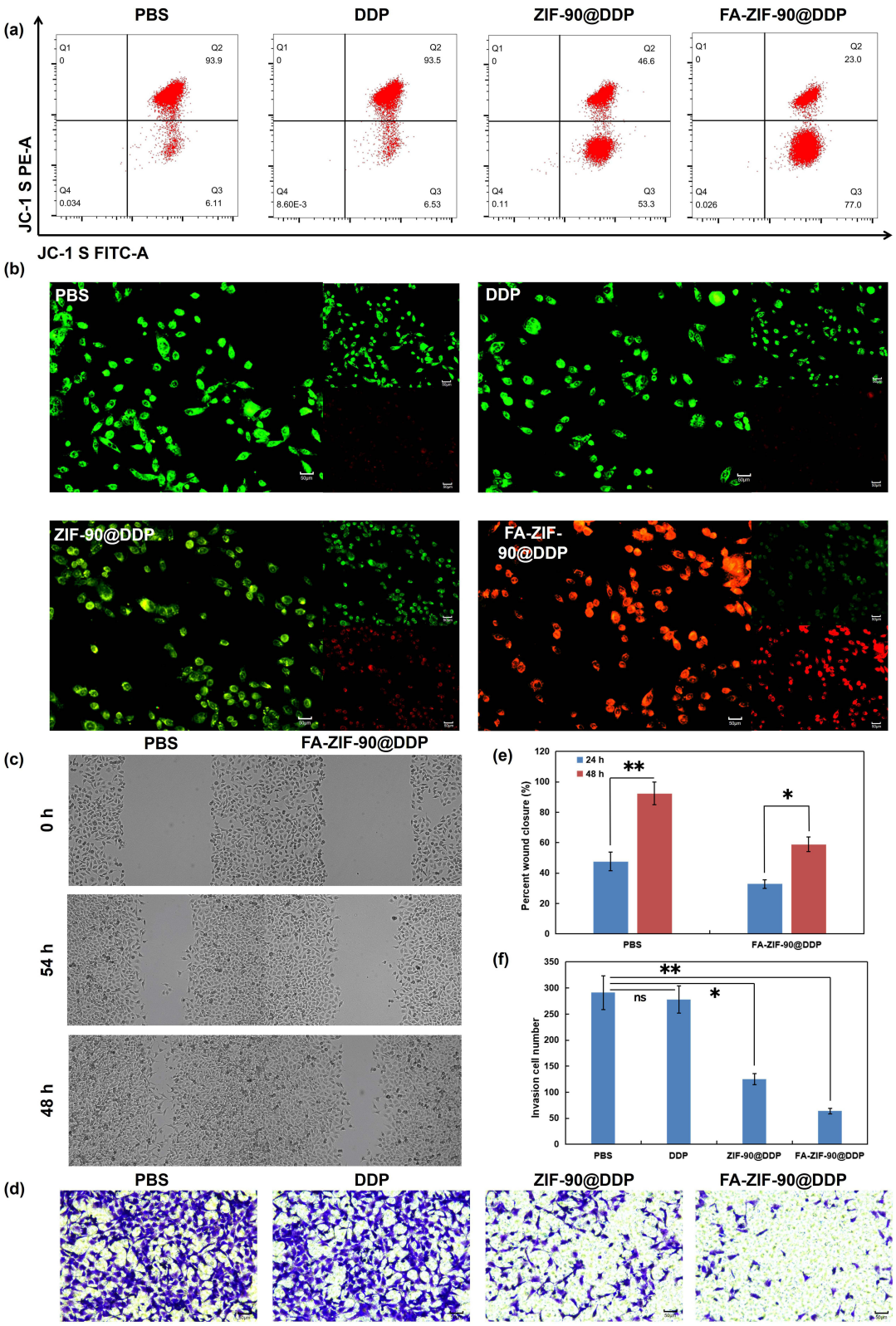

Figure 3 FA-ZIF-90@DDP interfered with mitochondrial changes and cell migration studies in A2780/DDP cells. (**a**) Results of mitochondrial membrane potential test after 8 h of different treatments of A2780/DDP cells with PBS, DDP, ZIF-90@DDP (DDP: 1 μg/mL), and FA-ZIF-90@DDP (DDP: 1 μg/mL) respectively. (**b**) Normal mitochondria (green) and inactivated mitochondria (red) were measured by confocal fluorescence microscopy (Scale bar = 50 μm). (**c**) Representative micrographs of wound healing in A2780/DDP cells after exposure to FA-ZIF-90@DDP (DDP: 1 μg/mL) or PBS at 0, 24, and 48 h. (**d**) Quantitative analysis of (**c**). (**e**) Results of statistical data analysis of migration capacity of A2780/DDP cells in (**f**). (**f**) Migration ability of A2780/DDP cells cultured on PBS, DDP, ZIF-90@DDP, and FA-ZIF-90@DDP. Data from wound healing and migration represent the mean ± SEM of three independent experiments. Statistical significance among groups: Not significant (ns), *P < 0.05, **P < 0.01.

activity, we designed a cell scratch assay to investigate whether this mitochondrial targeting also reduces the migration ability of cancer cells. The in vitro scratch assay is an important indicator for assessing cancer cell migration, and A2780/DDP cells are currently one of the most abundant cell types in the tissues of ovarian cancer patients, and their migratory ability is closely related to the metastasis and spread of ovarian cancer.[39–42] Cell migration was observed by scratching A2780/DDP cells. As evident in Figure 3c and d, quantitative analysis of the scratch width over time revealed that FA-ZIF-90@DDP nanoparticles significantly suppressed the migratory ability of ovarian cancer cells. Specifically, cells treated with FA-ZIF-90@DDP exhibited a wider scratch with less gap closure compared to PBS-treated control cells after the same duration. This demonstrates that FA-ZIF-90@DDP nanoparticles can effectively inhibit the motility and invasiveness of ovarian cancer cells. Meanwhile, as shown in Figure 3e and f, under the fixed field of view, the average number of migrated cells in the control, DDP, ZIF-90@DDP, and FA-ZIF-90@DDP groups were 295, 285, 130, and 70, respectively. Compared with the control group, FA-ZIF-90@DDP had the greatest inhibitory effect on the migration of A2780/DDP cells, followed by ZIF-90 @DDP and DDP. The results indicated that DDP encapsulated in FA-ZIF -90@DDP at the same concentration had a better inhibitory effect than encapsulated in ZIF-90@DDP or alone. The above results of inhibitory effect on A2780/DDP cell migration may be related to the overexpression of FA receptor in invasive cancer cells and the targeted binding of FA-modified ZIF-90@DDP for precise delivery of DDP to inhibit cancer cell metastasis.[43,44]

In this study, we initially verified that FA-ZIF-90@DDP nanomedicine could efficiently inhibit the mitochondrial activity of A2780/DDP cells, and this inhibition was closely related to its FA-modified antitumor activity, which provided a new idea for the development of highly targeted antitumor drug carriers. Follow-up work will be carried out to investigate the effect of inducing cell death and apoptosis in A2780/DDP cells in vitro.

In vitro Cytotoxicity of FA-ZIF-90@DDP

Comparison of the effects of FA-ZIF-90@DDP and ZIF-90@DDP nanomedicines on A2780/DDP cell viability (Figure 4a). It can be observed that both nanoparticles reduced cell survival and caused cell death with increasing platinum concentration. However, the cell-killing effect of FA-ZIF-90@DDP was significantly better than that of ZIF-90@DDP in the whole concentration range. The results showed that FA-ZIF-90@DDP was more effective in inducing cell death. To confirm the apoptosis-inducing effect, flow cytometry analysis was performed after treatment of A2780/DDP cells with different formulations. Compared to PBS and free DDP groups, nanoparticle-loaded drugs led to markedly higher apoptosis rates, with FA-ZIF-90@DDP showing the highest pro-apoptotic effect (Figure 4b). These quantitative results validate that nano-formulation, especially with FA-targeting, can significantly potentiate the apoptosis-inducing activity of DDP in resistant ovarian cancer cells. The apoptosis scatter plot also showed that the FA-ZIF-90@DDP group could distribute more cells in Q2 and Q3 apoptotic phases, which accounted for about 69.6% (Figure 4c). The above results confirmed that nanomedicines, especially FA-ZIF-90@DDP with mitochondria-targeting moiety, could significantly enhance the apoptosis-inducing effect on A2780/DDP cells by targeting drug introduction. To visually confirm the pro-apoptotic effects, fluorescence microscopy was utilized to examine the changes in apoptotic markers in A2780/DDP cells after treatment with different formulations (Figure 4d). The results showed that the PBS and DDP groups mainly showed green fluorescence, indicating that the cells had strong activity; the red fluorescence intensity of the FA-ZIF-90@DDP group was significantly enhanced while the green fluorescence was weakened, confirming that it could effectively induce apoptosis in A2780/DDP cells.

In summary, the two nanocarriers, especially FA-ZIF-90@DDP, could significantly induce tumor cell death or apoptosis. This may be related to the improved cellular uptake and mitochondrial localization of platinum-based drugs by the nanocarriers.[45–47] In particular, FA-ZIF-90@DDP showed enhanced apoptosis-inducing activity and significant clinical potential due to the high selectivity of its post-modified FA for tumors and their mitochondria, which allowed more drugs to enter tumor cells and damage mitochondria.[32,48,49] In vitro, tests of relevant mechanisms and therapeutic effects demonstrated FA-ZIF-90@DDP as a nanomedicine with the potential to be applied in vivo to inhibit drug resistance in ovarian cancer.

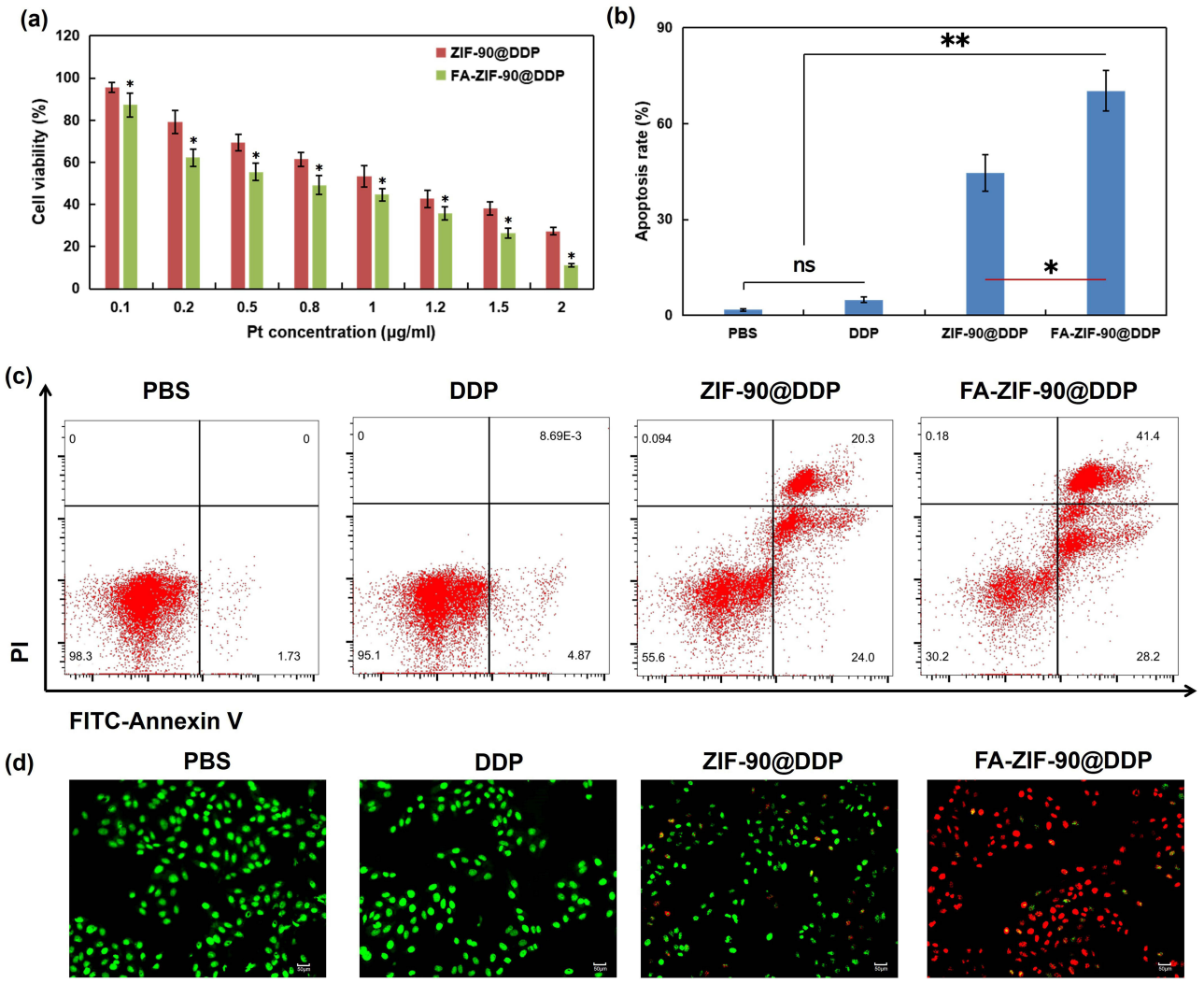

Figure 4 FA-ZIF-90@DDP induced cell death and apoptosis studies. (**a**) The viability of A2780/DDP cells was determined after 24 hours incubation with varying concentrations of non-targeted ZIF-90@DDP nanoparticles or folate receptor-targeted FA-ZIF-90@DDP nanoparticles using cell viability assays. (**b**) The apoptosis rate of A2780/DDP cells incubated with PBS, DDP, ZIF-90@DDP, and FA-ZIF-90@DDP for 24 h. (**c**) Flow cytometry analysis of apoptosis in A2780/DDP cells. Cells were treated with PBS, DDP, ZIF-90@DDP, and FA-ZIF-90@DDP for 24 h. Cells were stained with membrane-bound protein V-FITC/PI. (**d**) Confocal microscopic observation of apoptosis in A2780/DDP cells. Apoptosis of A2780/DDP cells incubated with PBS, DDP, ZIF-90@DDP, and FA-ZIF-90@DDP for 24 h (Scale bar = 50 μm). Data from cell experiment represent the mean ± SEM of three independent experiments. Statistical significance among groups: Not significant (ns), *P < 0.05.

In vivo Antitumor Effects of FA-ZIF-90

Encouraged by the above results, we further carried out tests on the in vivo anticancer effects of FA-ZIF-90/DDP. First, we compared the distribution of Pt concentration of drug carrier ZIF-90@DDP and FA-ZIF-90@DDP in different organs of mice (Figure 5a). This result showed that the highest accumulation of Pt was found in the liver, regardless of the DDP vector type. While in the heart, spleen, and kidney, there was little difference in Pt concentration distribution between the two carriers. However, in tumor tissues, FA-ZIF-90@DDP increased the Pt concentration by about 75% compared to the ZIF-90@DDP group, which demonstrated that the introduction of FA moiety significantly enhanced the tumor targeting of nanocarrier drugs. To assess the effect of FA-ZIF-90@DDP on tumor growth, we monitored the changes in tumor volume over time in mice in each administration group (Figure 5b). The results showed that, unlike the rapid increase in tumor volume in the PBS and DDP groups, both nano-loaded drugs significantly inhibited tumor proliferation, and in particular, the FA-ZIF-90@DDP group showed the most significant tumor-suppressive effect. This is consistent with the findings of high Pt concentration accumulation of FA-ZIF-90@DDP in tumor tissues in Figure 5a. Meanwhile, by affecting the body weight and survival rate of mice, we found that both nano-loaded drugs reduced the weight loss and

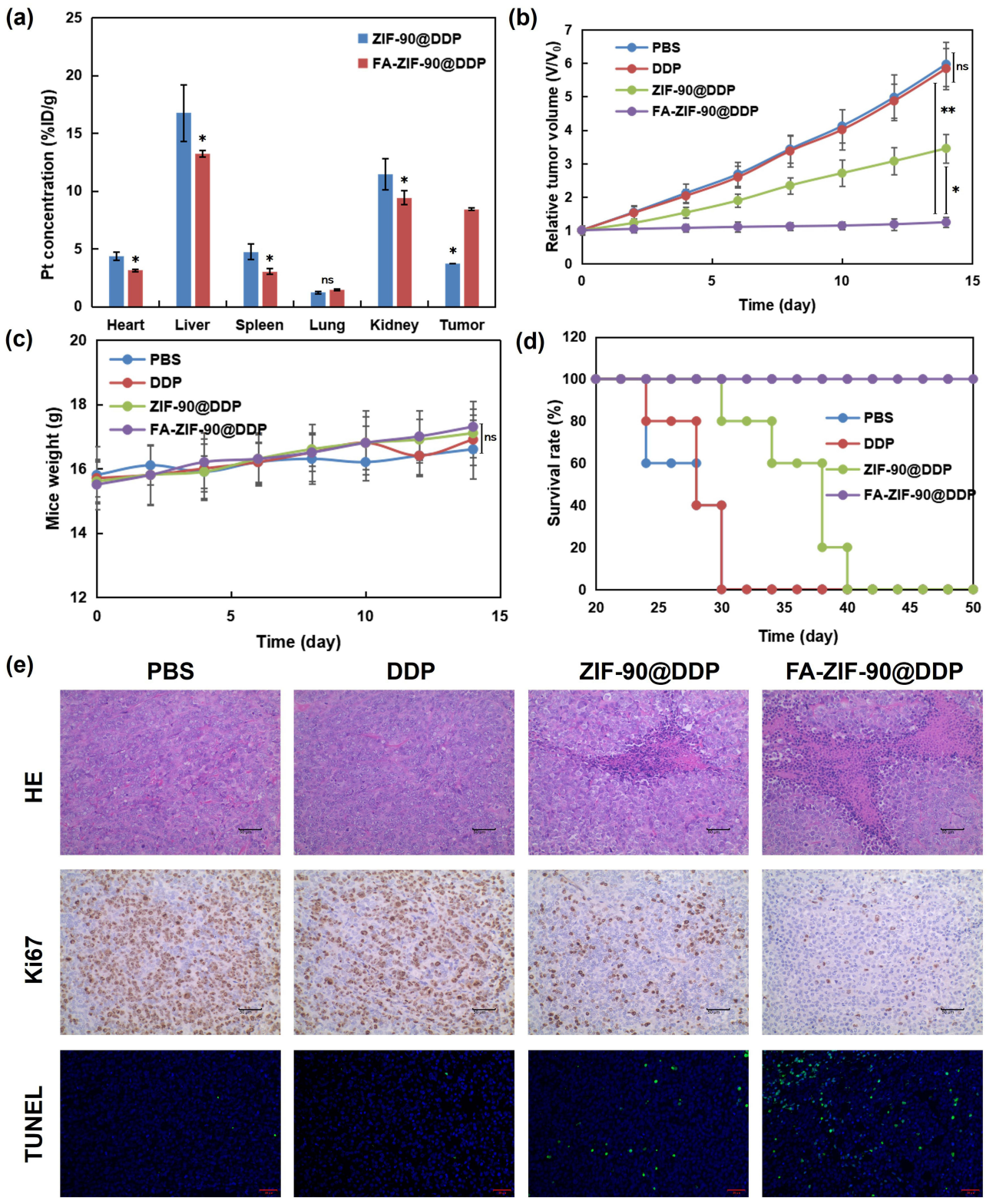

Figure 5 In vivo therapeutic effect study of FA-ZIF-90 @ DDP. (**a**) Biodistribution of mice with A2780/DDP human ovarian cancer tumors 24 h after intravesical injection of ZIF-90@DDP and FA-ZIF-90 @ DDP. (**b**) Relative tumor volume and, (**c**) body weight and, (**d**) survival rate of mice with loaded tumors after intravesical injection of PBS, DDP, ZIF-90@DDP, and ZIF-90@DDP. (**e**) H&E, ki67, and TUNEL staining of tumor sections after 24 h for a single treatment (Scale bar = 50 μm for H&E and Ki67, Scale bar = 20 μm for TUNEL). Data represent the mean ± SEM from five mice. Statistical significance among groups: Not significant (ns), *P < 0.05, **P < 0.01.

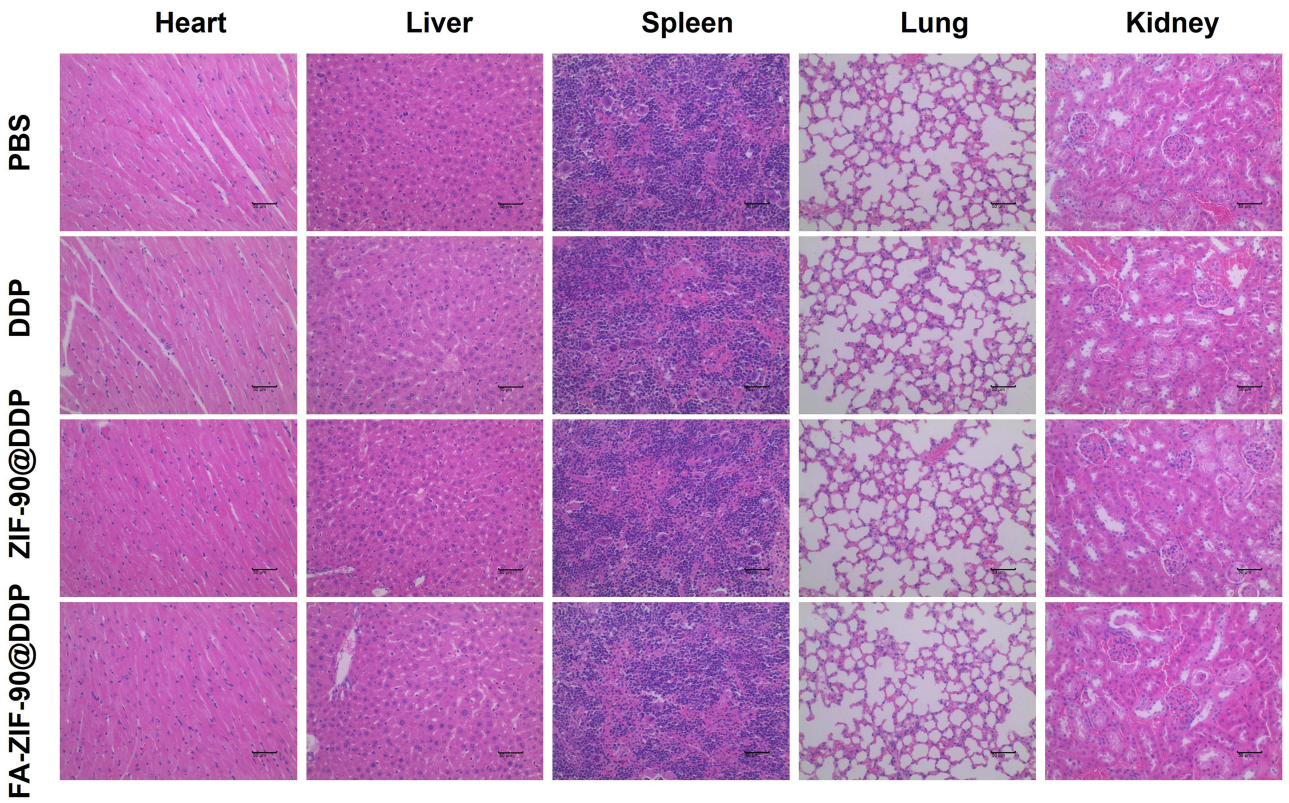

Figure 6 Effects of FA-ZIF-90@DDP on major organs. H&E staining of major organs of A2780/DDP hormonal mice after 14 days of different treatments (Scale bar = 50 μm).

increased the survival rate compared with the PBS and DDP groups, with FA-ZIF-90@DDP having the best effect (Figure 5c and d). During the observation period, the body weight of mice in the FA-ZIF-90@DDP group steadily increased to about 17 g, and the survival rate remained 100% at 50 days. The effects of different treatments on tumor tissues were subsequently evaluated using multiple staining (Figure 5e). H&E and TUNEL results showed that the two nano-loaded drugs increased tumor necrosis and apoptosis compared to the PBS and DDP groups. Ki67 immunohistochemistry results further confirmed that FA-ZIF-90@DDP significantly inhibited tumor cell proliferation. To assess the safety of different treatments, we examined the pathological changes in major organs (Figure 6). The results showed no significant differences between the groups, confirming that none of the different agents led to organ toxicity at the therapeutic dose. In conclusion, compared with ZIF-90@DDP and conventional DDP chemotherapy, FA-modified nanocarriers reduced toxic side effects, significantly prolonged mouse survival, presented excellent anti-tumor therapeutic effects, and is expected to be a highly effective and low-toxic tumor treatment strategy.[50–52]

Conclusion

In Conclusion, our study successfully established folate-conjugated ZIF-90 (FA-ZIF-90) as a sophisticated drug delivery system specifically designed to overcome cisplatin resistance in ovarian cancer. By integrating dual targeting - both to resistant cancer cells through folate receptor-mediated endocytosis and to mitochondria for direct intervention - FA-ZIF-90 effectively enhances tumour cell uptake, mitochondrial localisation of cisplatin and induces apoptosis, significantly outperforming non-targeted ZIF-90. The system's responsiveness to acidic pH and ATP within the tumour microenvironment ensures controlled and efficient release of cisplatin, thereby enhancing its chemotherapeutic effects. Our results highlight the potential of the FA-ZIF-90 platform to resensitise drug-resistant tumours to cisplatin therapy, offering a promising strategy to address the therapeutic challenges of ovarian cancer. Further elucidation of the underlying

molecular mechanisms and clinical translation studies are essential to fully realise the translational impact of this innovative approach in reversing chemoresistance and improving patient outcomes.

Acknowledgments

The authors acknowledge funding from the National Natural Science Foundation of China (32101153) and the Zhejiang Medical Health Science and Technology Project (2023KY264, 2024KY325). The authors also want to thank the Analysis & Testing Center at the Beijing Institute of Technology.

Disclosure

The authors declare that they have no known competing financial interests or personal relationships that could have appeared to influence the work reported in this paper.

References

1. Momenimovahed Z, Tiznobaik A, Taheri S, Salehiniya H. Ovarian cancer in the world: epidemiology and risk factors. *J Womens Health*. 2019;11:287–299. doi:10.2147/IJWH.S197604
2. Cabasag CJ, Arnold M, Rutherford M, et al. Shifting incidence and survival of epithelial ovarian cancer (1995-2014): a SurvMark-2 study. *Int, J, Cancer*. 2023;152(9):1763–1777. doi:10.1002/ijc.34403
3. Feng J, Xu L, Chen Y, Lin R, Li H, He H. Trends in incidence and mortality for ovarian cancer in China from 1990 to 2019 and its forecasted levels in 30 years. *J Ovarian Res*. 2023;16(1):139. doi:10.1186/s13048-023-01233-y
4. Chan DL, Morris DL, Rao A, Chua TC. Intraperitoneal chemotherapy in ovarian cancer: a review of tolerance and efficacy. *Cancer Manag Res*. 2012;413–422. doi:10.2147/CMAR.S31070
5. Świerczewska M, Sterzyńska K, Ruciński M, Andrzejewska M, Nowicki M, Januchowski R. The response and resistance to drugs in ovarian cancer cell lines in 2D monolayers and 3D spheroids. *Biomed Pharmacother*. 2023;165:115152. doi:10.1016/j.biopha.2023.115152
6. Liu J, Ma J, Zhang J, et al. Bibliometric and visualized analysis of drug resistance in ovarian cancer from 2013 to 2022. *Front Oncol*. 2023;13:1173863. doi:10.3389/fonc.2023.1173863
7. Qu J, Kamal MA, Yuan C. The regulatory roles of long non-coding RNA in the chemoresistance process of ovarian cancer. *Curr Pharm Des*. 2019;25(8):856–861. doi:10.2174/1381612825666190404122154
8. Amable L. Cisplatin resistance and opportunities for precision medicine. *Pharmacol Res*. 2016;106:27–36. doi:10.1016/j.phrs.2016.01.001
9. Emmings E, Mullany S, Chang Z, Landen CN Jr, Linder S, Bazzaro M. Targeting mitochondria for treatment of chemoresistant ovarian cancer. *Int J Mol Sci*. 2019;20(1):229. doi:10.3390/ijms20010229
10. Li X, Jiang H, He N, et al. Graphdiyne-related materials in biomedical applications and their potential in peripheral nerve tissue engineering. *Cyb Bion Sys*. 2022;2022. doi:10.34133/2022/9892526
11. Shen L, Zhan X. Mitochondrial dysfunction pathway alterations offer potential biomarkers and therapeutic targets for ovarian cancer. *Oxid Med Cell Longev*. 2022;2022:1.
12. Decollogne S, Joshi S, Chung SA, et al. Alterations in the mitochondrial responses to PENAO as a mechanism of resistance in ovarian cancer cells. *Gynecol Oncol*. 2015;138(2):363–371. doi:10.1016/j.ygyno.2015.06.018
13. Riganti C, Rolando B, Kopecka J, et al. Mitochondrial-targeting nitrooxy-doxorubicin: a new approach to overcome drug resistance. *Mol Pharm*. 2013;10(1):161–174. doi:10.1021/mp300311b
14. Xing Y, Jiang Z, Akakuru OU, et al. Mitochondria-targeting zeolitic imidazole frameworks to overcome platinum-resistant ovarian cancer. *Colloids Surf B*. 2020;189:110837. doi:10.1016/j.colsurfb.2020.110837
15. Alexandrova E, Pecoraro G, Sellitto A, et al. An overview of candidate therapeutic target genes in ovarian cancer. *Cancers*. 2020;12(6):1470. doi:10.3390/cancers12061470
16. Freund R, Zaremba O, Arnauts G, et al. The current status of MOF and COF applications. *Angew Chem Int Ed*. 2021;60(45):23975–24001.
17. Zhao C, Kang J, Li Y, et al. Carbon-based stimuli-responsive nanomaterials: classification and application. *Cyb Bion Sys*. 2023;4:0022. doi:10.34133/cbsystems.0022
18. Sun X, Keywanlu M, Tayebee R. Experimental and molecular dynamics simulation study on the delivery of some common drugs by ZIF-67, ZIF-90, and ZIF-8 zeolitic imidazolate frameworks. *Appl Organomet Chem*. 2021;35(11):e6377. doi:10.1002/aoc.6377
19. Lu L, Liu G, Lin C, et al. Mitochondrial metabolism targeted nanoplatform for efficient triple-negative breast cancer combination therapy. *Adv Healthc Mater*. 2021;10:undefined. doi:10.1002/adhm.202100978
20. Pan W, Cui B, Wang K, et al. ATP-triggered mitochondrial cascade reactions for cancer therapy with nanoscale zeolitic imidazole framework-90. *Theranostics*. 2021;11(16):7869. doi:10.7150/thno.59593
21. Jiang Z, Wang Y, Sun L, et al. Dual ATP and pH responsive ZIF-90 nanosystem with favorable biocompatibility and facile post-modification improves therapeutic outcomes of triple negative breast cancer in vivo. *Biomaterials*. 2019;197:41–50. doi:10.1016/j.biomaterials.2019.01.001
22. Yen C, Liu S, Lo W, et al. Cytotoxicity of postmodified zeolitic imidazolate framework-90 (ZIF-90) nanocrystals: correlation between functionality and toxicity. *Chem Eur J*. 2016;22(9):undefined. doi:10.1002/chem.201505005
23. Zhan G, Wang W, Sun H, Hou Y, Feng LJC, Systems B. Auto-csc: a transfer learning based automatic cell segmentation and count framework. *Cyb Bion Sys*. 2022;2022:1.
24. Cee VJ, Downing NS. A one-pot method for the synthesis of 2-aminobenzimidazoles and related heterocycles. *Tetrahedron Lett*. 2006;47 (22):3747–3750.
25. Han Z, Zhao Y, Jiang H, et al. (3-Aminopropyl) Triethoxysilane-Modified ZIF-90 nanoparticle/polydimethylsiloxane mixed matrix membranes for ethanol recovery via pervaporation. *ACS Appl Nano Mater*. 2021;5(1):183–194. doi:10.1021/acsanm.1c02523

26. Cao X, Liu S, Lu J, et al. Chitosan coated biocompatible zeolitic imidazolate framework ZIF-90 for targeted delivery of anticancer drug methotrexate. *J Solid State Chem*. 2021;300:122259. doi:10.1016/j.jssc.2021.122259
27. Patra CR, Bhattacharya R, Mukherjee P. Fabrication and functional characterization of goldnanoconjugates for potential application in ovarian cancer. *J Mater Chem A*. 2010;20(3):547–554.
28. Bax HJ, Chauhan J, Stavraka C, et al. Folate receptor alpha in ovarian cancer tissue and patient serum is associated with disease burden and treatment outcomes. *Br. J. Cancer*. 2023;128(2):342–353. doi:10.1038/s41416-022-02031-x
29. Young O, Ngo N, Lin L, et al. Folate receptor as a biomarker and therapeutic target in solid tumors. *Curr Probl Cancer*. 2023;47(1):100917. doi:10.1016/j.currproblcancer.2022.100917
30. Zhao H, Wei W, Sun Y, et al. Interference with the expression of β-catenin reverses cisplatin resistance in A2780/DDP cells and inhibits the progression of ovarian cancer in mouse model. *DNA Cell Biol*. 2015;34(1):55–62. doi:10.1089/dna.2014.2626
31. Kaur G, Shukla A, Sivakumar S, Verma S. Soft structure formation and cancer cell transport mechanisms of a folic acid–dipeptide conjugate. *J Pept Sci*. 2015;21(3):248–255. doi:10.1002/psc.2742
32. Wang S, Low PS. Folate-mediated targeting of antineoplastic drugs, imaging agents, and nucleic acids to cancer cells. *J Control Release*. 1998;53 (1–3):39–48. doi:10.1016/S0168-3659(97)00236-8
33. Vaidya B, Paliwal R, Rai S, et al. Cell-selective mitochondrial targeting: a new approach for cancer therapy. *J Cancer Ther*. 2009;7:1.
34. Wang J, Zhang L, Xin H, et al. Mitochondria-targeting folic acid-modified nanoplatform based on mesoporous carbon and a bioactive peptide for improved colorectal cancer treatment. *Acta Biomater*. 2022;152:453–472. doi:10.1016/j.actbio.2022.08.071
35. Narmani A, Rezvani M, Farhood B, et al. Folic acid functionalized nanoparticles as pharmaceutical carriers in drug delivery systems. *Drug Dev Res*. 2019;80(4):404–424. doi:10.1002/ddr.21545
36. Ai J-W, Liu B, Liu W-D. Folic acid-tagged titanium dioxide nanoparticles for enhanced anticancer effect in osteosarcoma cells. *Mater Sci Eng C*. 2017;76:1181–1187. doi:10.1016/j.msec.2017.03.027
37. Dong L, Gopalan V, Holland O, Neuzil J. Mitocans revisited: mitochondrial targeting as efficient anti-cancer therapy. *Int J Mol Sci*. 2020;21 (21):7941. doi:10.3390/ijms21217941
38. Yang Y, He P-Y, Zhang Y, Li N. Natural products targeting the mitochondria in cancers. *Molecules*. 2020;26(1):92. doi:10.3390/molecules26010092
39. Almeida VM, Bezerra MA, Nascimento JC, Amorim LMF. Anticancer drug screening: standardization of in vitro wound healing assay. *J Bras Patol Med Lab*. 2020;55:606–619.
40. Schmidt W, Chaney SG. Role of carrier ligand in platinum resistance of human carcinoma cell lines. *Cancer Res*. 1993;53(4):799–805.
41. Lu Y, Han J, Scanlon K. Biochemical and molecular properties of cisplatin-resistant A2780 cells grown in folinic acid. *J Biol Chem*. 1988;263 (10):4891–4894. doi:10.1016/S0021-9258(18)68869-6
42. Ma S, Liu D, Tan W, et al. Interference with SMO increases chemotherapy drug sensitivity of A2780/DDP cells by inhibiting the Hh/Gli signaling pathway. *J Cell Biochem*. 2020;121(5–6):3256–3265. doi:10.1002/jcb.29593
43. Allard JE, Risinger JI, Morrison C, et al. Overexpression of folate binding protein is associated with shortened progression-free survival in uterine adenocarcinomas. *Gynecol Oncol*. 2007;107(1):52–57. doi:10.1016/j.ygyno.2007.05.018
44. Chan KT, Choi MY, Lai KK, et al. Overexpression of transferrin receptor CD71 and its tumorigenic properties in esophageal squamous cell carcinoma. *Oncol Rep*. 2014;31(3):1296–1304. doi:10.3892/or.2014.2981
45. Wang X, Guo Z. Targeting and delivery of platinum-based anticancer drugs. *Chem Soc Rev*. 2013;42(1):202–224. doi:10.1039/C2CS35259A
46. Khoury A, Deo KM, Aldrich-Wright JR. Recent advances in platinum-based chemotherapeutics that exhibit inhibitory and targeted mechanisms of action. *J Inorg Biochem*. 2020;207:111070. doi:10.1016/j.jinorgbio.2020.111070
47. He C, Majd MH, Shiri F, Shahraki S. Palladium and platinum complexes of folic acid as new drug delivery systems for treatment of breast cancer cells. *J Mol Struct*. 2021;1229:129806. doi:10.1016/j.molstruc.2020.129806
48. Chen W-H, Xu X-D, Luo G-F, et al. Dual-targeting pro-apoptotic peptide for programmed cancer cell death via specific mitochondria damage. *Sci Rep*. 2013;3(1):3468. doi:10.1038/srep03468
49. Malhi SS, Budhiraja A, Arora S, et al. Intracellular delivery of redox cycler-doxorubicin to the mitochondria of cancer cell by folate receptor targeted mitocancerotropic liposomes. *Int J Pharm*. 2012;432(1–2):63–74. doi:10.1016/j.ijpharm.2012.04.030
50. Cheng X, Wang X, Cao Z, Yao W, Wang J, Tang R. Folic acid-modified soy protein nanoparticles for enhanced targeting and inhibitory. *Mater Sci Eng C*. 2017;71:298–307.
51. Cheng G, Song Z, Liu Y, et al. Long Noncoding RNA SNHG12 indicates the prognosis of prostate cancer and accelerates tumorigenesis via sponging MiR-133b. *J Cell Physiol*. 2020;235(2):1235–1246. doi:10.1002/jcp.29039
52. Vimala K, Shanthi K, Sundarraj S, Kannan S. Synergistic effect of chemo-photothermal for breast cancer therapy using folic acid (FA) modified zinc oxide nanosheet. *J Colloid Interface Sci*. 2017;488:92–108. doi:10.1016/j.jcis.2016.10.067